PCCP

ROYAL SOCIETY OF CHEMISTRY

PAPER

Cite this: *Phys. Chem. Chem. Phys.*, 2021, **23**, 2715

Effects of bending excitation on the reaction dynamics of fluorine atoms with ammonia

Li Tian,[ab] Hongwei Song *[a] and Minghui Yang [a]

Received 6th November 2020,
Accepted 22nd December 2020

DOI: 10.1039/d0cp05790h

rsc.li/pccp

Vibrational excitation has been established as an efficient way to control the chemical reaction outcome. Stretching vibration of polyatomic molecules is believed to be efficient to promote abstraction reactions since energy is placed directly into the breaking bond. In this work, we report on a counterexample showing that exciting the low-frequency umbrella bending mode of ammonia enhances its reaction with fluorine atoms much more than exciting the high-frequency symmetric or asymmetric stretching mode over a wide range of collision energy, validated using both quasiclassical trajectory simulations and full-dimensional quantum dynamics calculations under the centrifugal-sudden approximation. This interesting mode-specific reaction dynamic originates from the increased chance of capturing the fluorine atom by ammonia due to the enlarged attractive interaction between them and the enhancement of the direct stripping reaction mediated by two submerged barriers.

I. Introduction

Control of chemical reactions has long been a dream of chemists.[1–3] Traditionally, the rate or outcome of a reaction could be altered by changing the reaction environment or introducing a catalyst. With the advent of lasers, vibrational excitation of molecules has been becoming an intuitively appealing means of controlling chemistry.[1] The key to vibrational control of chemical reactions is exciting a vibration that maps significantly onto the reaction coordinate, in which the vibrational motion can be as simple as stretching a bond or as complex as a concerted motion of many atoms.[2–5]

Vibrational excitations of different reactant modes often possess different capacities in driving a bimolecular chemical reaction.[3,6–10] In most cases, this so called "mode specificity" can be well predicted using Polanyi's rules[11,12] for atom–diatom reactions or the sudden vector projection (SVP) model[13,14] for polyatomic reactions. Stretching excitation of polyatomic molecules is generally expected to enhance the reactivity more efficiently than bending excitation since vibrational energy is placed directly into the breaking bond. The effect of bending excitation on chemical reactions is not so intuitive.[15,16] Because the bending modes are of lower frequency and involve nonlocalized and concerted motions of three or more atoms, they do not obviously map onto the reaction coordinate. To date, the influence of bending excitation on chemical reactions remains ambiguous.

To the best of our knowledge, the efficacy of stretching excitation has been demonstrated to be almost higher than that of the bending excitation in promoting abstraction reactions, except at very low collision energies.[3] In the F + CD_4/CHD_3 and Cl + CH_4/CD_4 reactions, the bending excitation was proved to promote the reactivity at low collision energy while suppress the reactivity at high energy.[17–23] Herein, we present a counterexample that the excitation of the reactant umbrella mode significantly enhances the hydrogen abstraction reaction of fluorine atoms with ammonia, whose efficacy is remarkably higher than exciting either of the two stretching modes of ammonia over a wide range of collision energy. This peculiar mode specificity is attributed to the enhanced occurrence of direct reaction by exciting the umbrella mode, which is mediated by two sequential submerged barriers along the minimum energy path (MEP).

The $F(^2P) + NH_3 \rightarrow HF + NH_2$ reaction takes place very fast by overcoming two shallow submerged barriers, and is accompanied by an even faster secondary hydrogen abstraction reaction $F + NH_2 \rightarrow HF + NH$, which poses a big challenge to both theoretical and experimental studies.[24–27] Much attention has been paid to investigate its kinetics and dynamics.[28–32] Espinosa-Garcia and Corchado developed a full-dimensional analytical potential energy surface (PES),[33] on which the calculated differential cross sections agreed reasonably well with the experimental results while the agreement of calculated product energy partitions with experimental values was

[a] *State Key Laboratory of Magnetic Resonance and Atomic and Molecular Physics, Wuhan Institute of Physics and Mathematics, Innovation Academy for Precision Measurement Science and Technology, Chinese Academy of Sciences, Wuhan 430071, China. E-mail: hwsong@wipm.ac.cn*

[b] *College of Physical Science and Technology, Huazhong Normal University, Wuhan 430079, China*

slightly poor.[34,35] The poor agreement was ascribed to the excessively attractive character of the stretching terms in the analytical expression of the PES. Recently, we constructed a new PES by fitting 41 282 *ab initio* energy points at the level of UCCSD(T)-F12/aug-cc-pVTZ.[36] Thanks to the flexibility of the fundamental invariant-neural network method,[37–39] the PES has a total root mean square error of 0.13 kcal mol^{-1}. The calculated differential cross sections and product energy partitions both reproduced well the experimental results, validating the accuracy of the PES.

In this work, quasi-classical trajectory (QCT) and initial state-selected time-dependent quantum wave packet methods are employed to study the mode-specific dynamics of the reaction F + NH_3 → HF + NH_2 on a newly developed *ab initio*-based PES.[36] The vibrational states of the reactant NH_3 are designated by (ν_1, ν_2, ν_3, and ν_4), in which the four quantum numbers denote excitations in the four normal modes: symmetric stretching, umbrella (symmetric bending), asymmetric stretching, and asymmetric bending, respectively. Due to the existence of an inversion barrier, there exist two components for the umbrella mode of NH_3: the lower symmetric and upper antisymmetric components. This work focuses on the lower symmetric component since no discernible difference for the reaction probability was found between the tunneling pair in the hydrogen abstraction reaction between the hydrogen atom and ammonia.[40,41]

II. Theory

A. Quantum dynamics

The initial state-selected time-dependent quantum wave packet method has been detailed in the literature.[42–45] Here, we introduce briefly the aspects relevant to this work. The full-dimensional Hamiltonian for the penta-atomic system X + YABC in the reactant Jacobi coordinates with a given total angular momentum $J_{\rm tot}$ can be written as ($\hbar$ = 1 hereafter):[40,46,47]

$$\begin{aligned}\hat{H} &= -\frac{1}{2\mu_{\rm R}}\frac{\partial^2}{\partial R^2}-\frac{1}{2\mu_1}\frac{\partial^2}{\partial r_1^2}-\frac{1}{2\mu_2}\frac{\partial^2}{\partial r_2^2}\\ &\quad-\frac{1}{2\mu_3}\frac{\partial^2}{\partial r_3^2}+\frac{(\hat{J}_{\rm tot}-\hat{J})^2}{2\mu_{\rm R}R^2}+\frac{\hat{l}_1^2}{2\mu_1 r_1^2}\\ &\quad+\frac{\hat{l}_2^2}{2\mu_2 r_2^2}+\frac{\hat{j}_3^2}{2\mu_3 r_3^2}+\hat{V}(R,r_1,r_2,r_3,\theta_1,\theta_2,\theta_3,\varphi_1,\varphi_2),\end{aligned} \tag{1}$$

where $\boldsymbol{R}$ is the Jacobi vector from the center of mass (COM) of YABC to the atom X, $\boldsymbol{r}_1$ is the vector from the COM of ABC to the atom Y, $\boldsymbol{r}_2$ is the vector from the COM of BC to the atom A, and $\boldsymbol{r}_3$ is the vector from the atom C to the atom B, with $\mu_{\rm R}$, μ_1, μ_2 and μ_3 as their corresponding reduced masses. $\hat{j}_3$ is the rotational angular momentum operator of the moiety BC and $\hat{l}_2$ is the orbital angular momentum operator along r_2. The coupling of $\hat{j}_3$ and $\hat{l}_2$ gives rise to $\hat{j}_{23}$. $\hat{l}_1$ is the orbital angular momentum operator along $\boldsymbol{r}_1$, and its coupling with $\hat{j}_{23}$ generates $\hat{J}$. $\hat{J}_{\rm tot}$ is the total angular momentum operator of the system.

The parity (ε) adapted wave function is expanded in terms of the body-fixed (BF) ro-vibrational basis functions:

$$\begin{aligned}\psi^{J_{\rm tot}M\varepsilon}(R,r_1,r_2,r_3) &= \sum_{n,\nu,j,K} C_{n\nu jK}^{J_{\rm tot}M\varepsilon} u_n^{\nu_1}(R)\varphi_{\nu_1}(r_1)\varphi_{\nu_2}(r_2)\varphi_{\nu_3}(r_3)\\ &\quad\times\ \Phi_{jK}^{J_{\rm tot}M\varepsilon}(\hat{R},\hat{r}_1,\hat{r}_2,\hat{r}_3),\end{aligned} \tag{2}$$

where $C_{n\nu jK}^{J_{\rm tot}M\varepsilon}$ are time-dependent coefficients. $u_n^{\nu_1}(R)$ are sine translational basis functions. ν denotes the vibrational basis indices (ν_1,ν_2,ν_3), and $\varphi_{\nu_i}(r_i)$ is obtained by solving the one-dimensional (1D) reference Hamiltonian defined as

$$\hat{h}_i(r_i) = -\frac{1}{2\mu_i}\frac{\partial^2}{\partial r_i^2}+V_i^{\rm ref}(r_i),\quad i=1,3 \tag{3}$$

where $V_i^{\rm ref}(r_i)$ is the corresponding 1D reference potential. j represents (l_1,l_2,j_3,j_{23},J). $\Phi_{jK}^{J_{\rm tot}M\varepsilon}$ in eqn (2) is the parity-adapted coupled BF total angular momentum eigenfunction, which can be written as[46]

$$\begin{aligned}\Phi_{jK}^{J_{\rm tot}M\varepsilon} &= (1+\delta_{K0})^{-1/2}\sqrt{\frac{2J_{\rm tot}+1}{8\pi}}\\ &\quad\times\ \left[\bar{D}_{K,M}^{J_{\rm tot}}Y_{l_1j_{23}l_2j_3}^{JK}+\varepsilon(-1)^{l_1+l_2+j_3+J+J_{\rm tot}}\bar{D}_{-K,M}^{J_{\rm tot}}Y_{l_1j_{23}l_2j_3}^{J-K}\right],\end{aligned} \tag{4}$$

where $D_{K,M}^{J}$ is the Wigner rotation matrix.[48] M is the projection of $J_{\rm tot}$ on the space-fixed z axis. K is the projection of $J_{\rm tot}$ on the BF z axis, which is defined to coincide with the vector $\boldsymbol{R}$. $Y_{l_1j_{23}l_2j_3}^{JK}$ is the eigenfunction of the angular momentum operator $\hat{J}$, which is defined as

$$Y_{l_1j_{23}l_2j_3}^{JK} = \sum_{\omega}\bar{D}_{K\omega}^{J}(r_1)\sqrt{\frac{2l_1+1}{2J+1}}\langle j_{23}\omega l_1 0\mid J\omega\rangle Y_{j_{23}l_2j_3\omega}(\hat{r}_2,\hat{r}_3), \tag{5}$$

and

$$Y_{j_{23}l_2j_3\omega}(\hat{r}_2,\hat{r}_3) = \sum_{m}\bar{D}_{\omega m}^{j_{23}}(\hat{r}_2)\sqrt{\frac{2l_2+1}{2j_{23}+1}}\langle j_3 m l_2 0\mid j_{23}m\rangle y_{j_3m}(\hat{r}_3), \tag{6}$$

where y_{jm} denotes the spherical harmonics. Note the restriction that $\varepsilon(-1)^{l_1+l_2+j_3+J+J_{\rm tot}}=0$ for $K=0$ in eqn (4).

To save the computational effort, the centrifugal-sudden (CS) approximation[49,50] is applied in the calculations. Under the CS approximation, the coupling between different K blocks is neglected. The centrifugal term, $(\hat{J}_{\rm tot}-\hat{J})^2$, is thus approximated using

$$\begin{aligned}&\left\langle\Phi_{jK}^{J_{\rm tot}M\varepsilon}\middle|(\hat{J}_{\rm tot}-\hat{J})^2\middle|\Phi_{j'K'}^{J_{\rm tot}M\varepsilon}\right\rangle\\ &\quad\approx\delta_{jj'}\delta_{KK'}\left[J_{\rm tot}(J_{\rm tot}+1)+J(J+1)-2K^2\right].\end{aligned} \tag{7}$$

The initial wave packet $|\chi_i\rangle$ is built by the direct product of a Gaussian wave packet along the scattering coordinate $\boldsymbol{R}$ and a specific ro-vibrational state of the reactant NH_3 in the BF representation:

$$|\chi_i\rangle = \left(\frac{1}{\pi\delta^2}\right)^{\frac{1}{4}}e^{-(R-R_0)^2/2\delta^2}e^{-ik_0R}|\nu_0 j_0\tau;JK\varepsilon\rangle, \tag{8}$$

where R_0 and δ are the mean position and the width of the initial Gaussian function and $k_0 = \sqrt{2\mu_R E_i}$ is the mean momentum. The eigenfunctions of NH_3 are obtained by diagonalizing its six-dimensional Hamiltonian in the reactant asymptote. The three quantum numbers, ν_0,j_0 and τ, denote the initial vibrational state, total angular momentum and parity of NH_3, respectively. The second-order split-operator method[51] is implemented to propagate the wave packet. To impose outgoing boundary conditions, the following negative imaginary absorbing potentials F are applied at the grid edges:[52]

$$F(x) = -i\alpha\left(\frac{x - x_s}{x_{max} - x_s}\right)^n, \quad (9)$$

where $x = R$, and r_1, x_s is the starting point of the absorbing potential, and x_{max} is the end of the grid.

The total reaction probability from a specific initial state is calculated by

$$P^{J_{tot}\varepsilon}_{\nu_0 j_0 \tau K_0}(E) = \langle \chi_i^+(E)|\hat{F}|\chi_i^+(E)\rangle, \quad (10)$$

in which the flux through the dividing surface $S(r_1 = r_1^F)$ is calculated from the energy-dependent scattering wavefunction that is obtained by Fourier transforming the wave packet on the dividing surface.[53]

The total reaction integral cross section (ICS) from a specific initial state is computed by summing the reaction probabilities over all relevant partial waves:

$$\sigma_{\nu_0 j_0 \tau}(E) = \frac{1}{(2j_0+1)}\sum_{K_0\varepsilon}\frac{\pi}{k^2}\sum_{J_{tot}\geq K_0}(2J_{tot}+1)P^{J_{tot}\varepsilon}_{\nu_0 j_0 \tau K_0}(E). \quad (11)$$

Since we are only interested in the vibrational state-specific dynamics in this work, the angular momentum index will be dropped hereafter.

The quantum scattering calculations are performed on an L-shaped grid.[54] For the scattering coordinate R, 136 sine discrete variable representation (DVR) basis/points[55] are used in the whole range from 2.5 to 11.0 a_0 and 68 sine DVR basis/points are used in the interaction region. For the dissociating coordinate r_1, 31 potential optimized DVR (PODVR) basis/points[56] are used in the interaction region and 2 PODVR basis/points are used in the asymptotic region. 2 PODVR basis/points are used along the coordinates r_2 and r_3. The propagation time is around 25 000 a.u. with a time step of 10 a.u.

B. Quasi-classical trajectory method

The software VENUS[57] is implemented to perform standard QCT calculations on the same PES. The total ICS is calculated using

$$\sigma_r(E_c) = \pi b_{max}{}^2\frac{N_r}{N_t}, \quad (12)$$

where N_r and N_t denote the numbers of reactive and total trajectories, respectively. b_{max} is the maximal impact parameter that is determined using small batches of trajectories with trial values at each initial state. The impact parameter b is sampled by $b = R^{1/2}b_{max}$, where R is a uniform random number in [0,1]. The statistical error is given by $\Delta = \sqrt{(N_t - N_r)/N_t N_r}$.

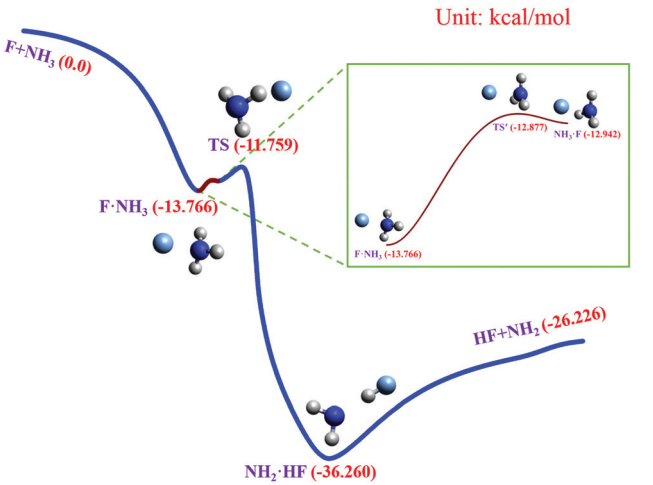

Fig. 1 Schematic diagram of the reaction path for the F + NH_3 → HF + NH_2 reaction.

The differential cross section (DCS) is calculated using

$$\frac{d\sigma_r}{d\Omega} = \frac{\sigma_r P_r(\theta)}{2\pi\sin(\theta)}, \quad (13)$$

where $P_r(\theta)$ is the normalized reaction probability with the scattering angle θ defined as

$$\theta = \cos^{-1}\left(\frac{\vec{\nu}_i \cdot \vec{\nu}_f}{|\vec{\nu}_i| \cdot |\vec{\nu}_f|}\right), \quad (14)$$

in which $\vec{\nu}_i = \vec{\nu}_F - \vec{\nu}_{NH_3}$ and $\vec{\nu}_f = \vec{\nu}_{HF} - \vec{\nu}_{NH_2}$.

The initial states of NH_3 are sampled using a harmonic normal mode sampling. These states are not the stationary states of the real molecular Hamiltonian due to the energy flow among the vibrational modes. However, the normal mode sampling could provide reasonable results when the harmonic action is averaged over an ensemble of trajectories. One alternative is to use a semiclassical method like adiabatic switching.[58] The vibrational state of the product HF is determined using the Einstein–Brillouin–Keller semiclassical quantization[59] of the action integral while the vibrational state distribution of NH_2 is obtained using the normal mode analysis (NMA) method proposed by Corchado and Espinosa–García.[60,61] In this work, the coordinates and momenta of each reactive trajectory are extracted from a specific step within the last vibrational period of the product molecules, for which the corresponding geometry required to have the lowest potential energy within the vibrational period, guaranteeing, at least to some extent, the accuracy of the harmonic approximation.[62] If the chosen geometry departs from the corresponding equilibrium geometry far away, the harmonic approximation possibly breaks down, resulting in unreliable classical action numbers. Two binning methods, namely histogram binning (HB)[63] and energy-based Gaussian binning (1GB),[64,65] are implemented to confer a ''quantum spirit'' on the noninteger

classical harmonic action number. For the 1GB method applied in this work, a 1GB weight for each product is implemented in the statistics.

Batches of trajectories (80 000–200 000) are run from each initial state with the collision energy taken from 1 kcal mol^{-1} to 23 kcal mol^{-1}. The statistical errors are all below 0.5%. The initial vibrational states of NH_3 are sampled using the fixed normal mode method. The trajectories are launched with a reactant separation of 8.0 Å and terminated when products or reactants reach a separation of 8.0 Å for reactive or non-reactive trajectories. The time step is selected to be 0.01 fs and the energy is conserved better than 10^{-4} kcal mol^{-1}.

III. Results and discussion

Fig. 1 shows the schematic diagram of the reaction path. There exists a submerged transition state (TS) in between the pre- and post-reaction wells. The transition state TS has a C_s symmetry with the fluorine atom pointing at one of the hydrogen atoms in the reactant NH_3. Interestingly, as shown in the inset, the reaction required to overcome an inversion barrier TS′ with C_{3v} symmetry when going through the pre-reaction well, like the famous Walden inversion favored by S_N2 reactions.[66,67] Although some dynamics studies demonstrated that the submerged barriers play a vital role in the rotational enhancement effect,[68–73] they are usually expected to have little effect on the vibrational mode-specific dynamics due to the negative barrier heights.

The calculated QCT and QD integral cross sections from the ground and fundamental states of the reactant NH_3 are presented in Fig. 2. The QD calculations launched from the fundamentals of the asymmetric stretching (ν_3) and asymmetric bending (ν_4) modes are prohibitive due to the extremely huge computational cost, and thus the corresponding ICSs are not presented here. The QCT ICS from each state initially decreases sharply and then levels off with the increase of collision energy, satisfying the character of a barrier-less reaction. Vibrational excitations all promote the reaction while their efficacies are disparate. Surprisingly, the umbrella mode (ν_2) has the highest efficacy in promoting the reaction compared to the other three normal modes. Note that the frequencies of the four modes (ν_1, ν_2, ν_3, and ν_4) are 3336.11, 932.43, 3443.07, and 1626.30 cm^{-1}, respectively. It means that the reactivity can be effectively enhanced by exciting the low-frequency umbrella mode. In contrast, the efficacies of two high-frequency stretching modes (ν_1 and ν_3) are less pronounced, which are even lower than that of the asymmetric bending mode (ν_4). The remarkably higher efficacy of the umbrella mode is confirmed by the full-dimensional QD calculations. The QD ICS from the ν_2 fundamental is significantly larger than the ICS from either the ground state or the ν_1 fundamental state, except at very collision energies where there exist strong oscillations.

Fig. 3a depicts the contours of the PES as a function of the bond distance F–N and the umbrella angle of NH_3 with the other coordinates fixed at the geometry of the transition state TS. The reaction mostly takes place by going through the pre-reaction wells. When the umbrella mode is excited, the umbrella angle will be enlarged compared with the angle along the minimum energy path. The attractive interaction, as shown

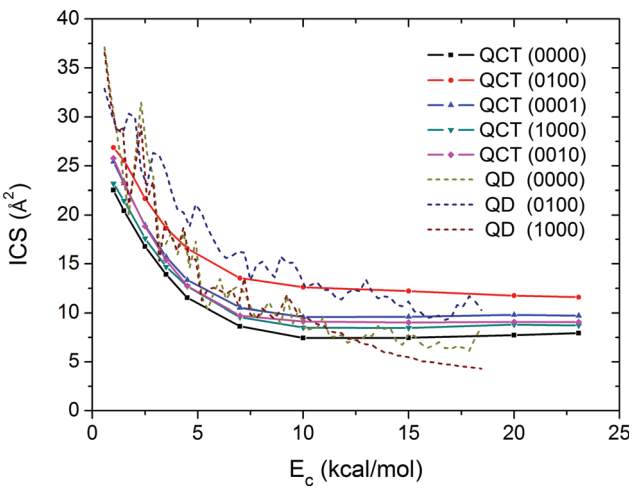

Fig. 2 QCT and QD integral cross sections of the reaction from the ground and fundamentals of NH_3 vibrational modes.

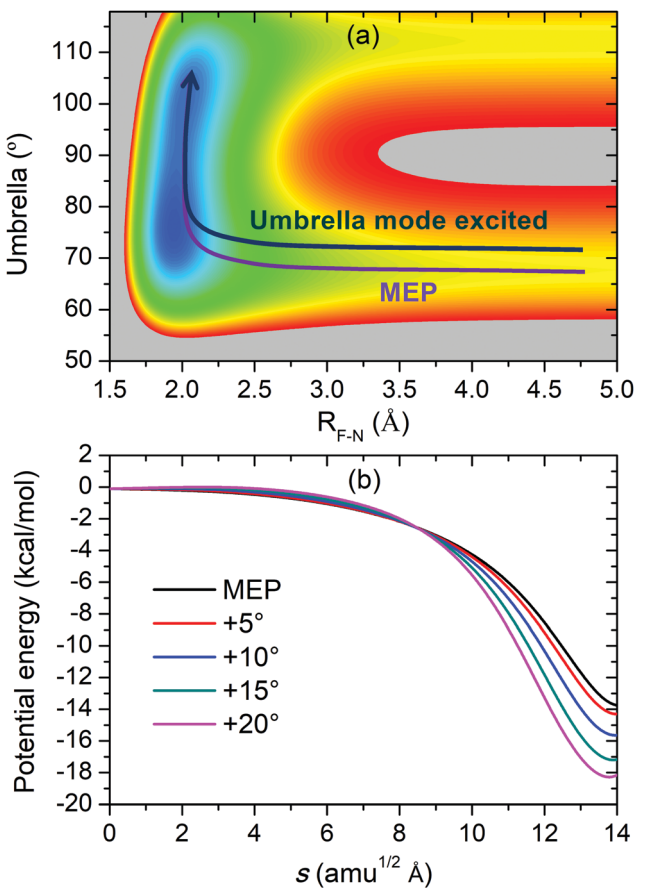

Fig. 3 (a) Contours of the PES as a function of the bond distance F–N and the umbrella angle of NH_3; (b) potential energy change along the MEP at different umbrella angles.

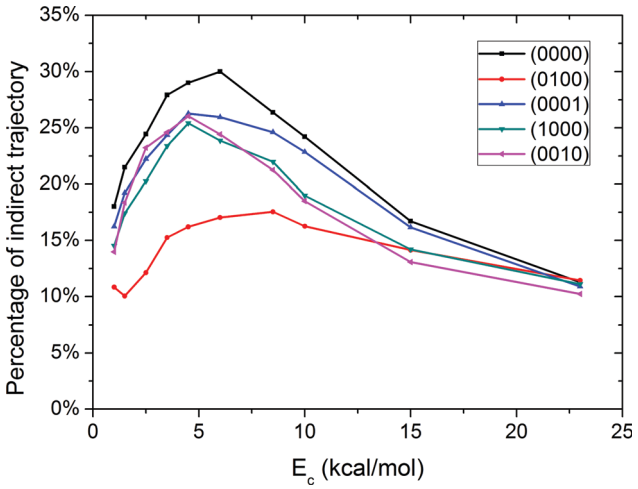

Fig. 4 Ratio of indirect reactive trajectories to total reactive trajectories for the reaction from the ground and fundamentals of NH_3 vibrational modes.

in Fig. 3b, is strengthened, which increases the chance of capturing the fluorine atom by the ammonia, thus of passing through the submerged barrier.

The reaction was found in previous studies to be dominated by the direct stripping and rebound mechanisms. The indirect "yo–yo" mechanism, resulting largely from the pre-reaction well, made a considerable amount of contribution.[34,36] Fig. 4 shows the ratio of indirect reactive trajectories to total reactive trajectories from different initial states. The trajectories for which either the forming bond HF or the breaking bond NH has large amplitude vibrations for more than one period are considered to take place by an indirect mechanism. When the umbrella mode of NH_3 is fundamentally excited, the percentage of indirect trajectories visibly decreases at low and moderate collision energies, indicating that exciting the umbrella mode leads to the occurrence of a direct reaction. The percentage of indirect trajectory appears to be insensitive to the initial state at high collision energy. As the collision energy increases, the indirect mechanism is further suppressed, making the separation of direct and indirect trajectories somewhat ambiguous.

The reaction probability is plotted as a function of impact parameter in Fig. 5 with the collision energy E_c fixed at 4.5, 10.0, 15.0 and 23.0 kcal mol^{-1}. The reaction probability is mainly enhanced by large impact-parameter collisions when the umbrella mode is excited. The corresponding differential cross sections are plotted in Fig. 6. The forward scattering is visibly enhanced when exciting the umbrella mode, corresponding to the large impact-parameter collisions in Fig. 5. Therefore, the enhancement effect of the umbrella mode excitation is to a large extent caused by the direct stripping mechanism, no matter at low and high collision energies. Exciting the umbrella mode facilitates the occurrence of the direct stripping reaction.

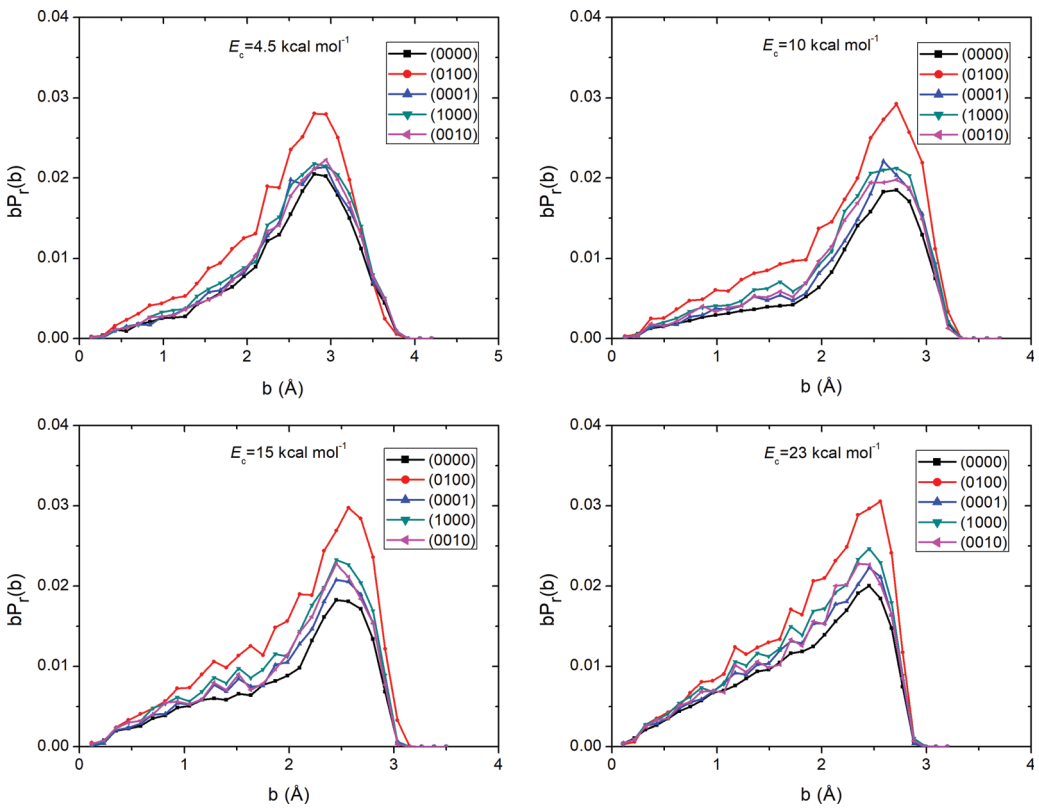

Fig. 5 Reaction probability of the F + NH_3 → HF + NH_2 reaction as a function of impact parameter b from the ground and fundamentals of NH_3 vibrational modes with the collision energy E_c = 4.5, 10.0, 15.0 and 23.0 kcal mol^{-1}.

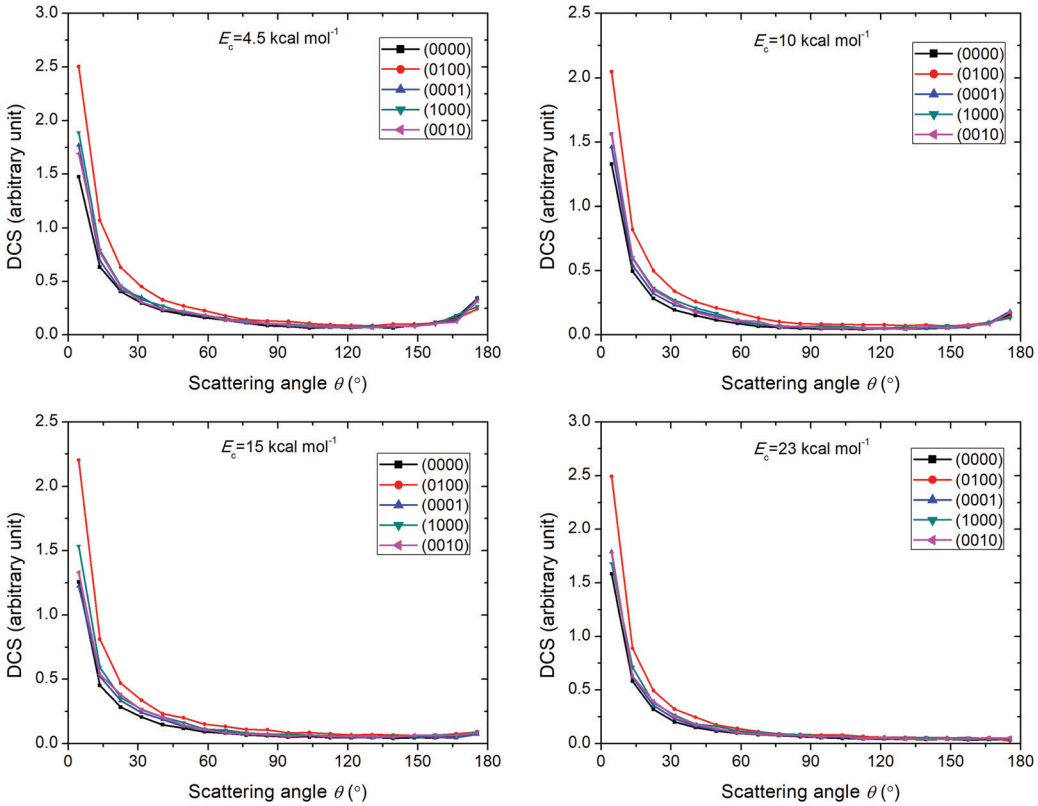

Fig. 6 Differential cross sections of the F + NH_3 → HF + NH_2 reaction from the ground and fundamentals of NH_3 vibrational modes with the collision energy E_c = 4.5, 10.0, 15.0 and 23.0 kcal mol^{-1}.

As was stated above, the remarkable promotional effect of exciting the umbrella on the reactivity is largely caused by the enhancement of the direct reaction. If so, the submerged barriers are expected to play a pivotal role in the observed mode selectivity. It is readily understandable that excitation of the umbrella mode facilitates the reaction to overcome the first inversion barrier (TS′). However, the effect of the second submerged barrier (TS) is not so intuitive as the umbrella mode involves concerted motion of three H atoms and the transition state TS possesses a C_s symmetry with the fluorine atom pointing at one of the three H atoms. The SVP model[13,14] is utilized to rationalize the effect of the second transition state (TS) on controlling the reaction. In the SVP model, the efficacy of a reactant mode in enhancing a reaction is attributed to its coupling with the reaction coordinate at the transition state, which is semi-quantitatively defined by the projection of the reactant normal mode vector ($\vec{Q}_i$) onto the reaction coordinate vector ($\vec{Q}_{RC}$) at the transition state: $P_i = \vec{Q}_i \cdot \vec{Q}_{RC} \in [0,1]$.[13] For the direct reaction, the collision time is assumed to be much faster than the intramolecular vibrational energy redistribution of NH_3. The calculated SVP values are listed in Table 1. The umbrella mode has the largest projection, followed by the asymmetric and symmetric stretching modes. These values imply that exciting the umbrella mode is much more efficient than exciting the two stretching modes, in good agreement with QD and QCT calculations. By contrast, the asymmetric bending mode has a tiny projection on the reaction coordinate while QCT calculations show that exciting the asymmetric bending mode is slightly more efficient than the two stretching modes in promoting the reaction. Note that the SVP model sometimes has difficulties to predict the efficacy of low-frequency bending modes.[14]

Table 1 SVP values for the F + NH_3 → HF + NH_2 reaction

Mode	SVP
ν_1 (symmetric stretch)	0.117
ν_2 (umbrella)	0.334
ν_3 (asymmetric stretch)	0.135
ν_4 (asymmetric bending)	0.044
Translational	0.038

IV. Conclusions

The dynamics of the hydrogen abstraction reaction between F and NH_3 has been studied using the QCT and full-dimensional QD methods on a recently developed *ab initio*-based PES. Exciting the low-frequency umbrella bending mode of NH_3 promotes the reactivity remarkably more than exciting the high-frequency symmetric or asymmetric stretching mode over the collision energy studied, which is considered to be a counterexample to the general opinion that the efficacy of stretching excitation is higher than that of the bending

excitation in promoting abstraction reactions. This interesting dynamical behavior is attributed to, on the one hand, the enlarged attractive interaction between F and NH_3, which increases the chance of capturing F by NH_3, and on the other hand, the modulation of the two submerged barriers, for which exciting the umbrella mode enhances the direct reaction. Since there exist submerged barriers in many radical-radical and ion–molecule reactions, it is highly desirable to explore the effect of bending excitation on these reactions. It is our hope that the theoretical predictions will stimulate experimental exploration of mode specific dynamics in these kinds of reactions.

Conflicts of interest

Authors declare no conflict of interest.

Acknowledgements

This work was supported by the National Natural Science Foundation of China (Grant No. 21973109 to HS, and 21773297 and 21973108 to MY).

References

1 R. N. Zare, *Science*, 1998, **279**, 1875–1879.
2 F. F. Crim, *Acc. Chem. Res.*, 1999, **32**, 877–884.
3 K. Liu, *Annu. Rev. Phys. Chem.*, 2016, **67**, 91–111.
4 F. F. Crim, *J. Phys. Chem.*, 1996, **100**, 12725–12734.
5 H. Guo and K. Liu, *Chem. Sci.*, 2016, **7**, 3992–4003.
6 D. C. Clary, *J. Phys. Chem.*, 1994, **98**, 10678–10688.
7 G. Czakó and J. M. Bowman, *J. Phys. Chem. A*, 2014, **118**, 2839–2864.
8 R. Welsch and U. Manthe, *J. Chem. Phys.*, 2014, **141**, 051102.
9 D. H. Zhang and H. Guo, *Annu. Rev. Phys. Chem.*, 2016, **67**, 135–158.
10 B. Fu, X. Shan, D. H. Zhang and D. C. Clary, *Chem. Soc. Rev.*, 2017, **46**, 7625–7649.
11 J. C. Polanyi, *Acc. Chem. Res.*, 1972, **5**, 161–168.
12 J. C. Polanyi, *Science*, 1987, **236**, 680–690.
13 B. Jiang and H. Guo, *J. Chem. Phys.*, 2013, **138**, 234104.
14 H. Guo and B. Jiang, *Acc. Chem. Res.*, 2014, **47**, 3679–3685.
15 M. J. Bronikowski, W. R. Simpson and R. N. Zare, *J. Phys. Chem.*, 1993, **97**, 2204–2208.
16 S. A. Kandel and R. N. Zare, *J. Chem. Phys.*, 1998, **109**, 9719–9727.
17 J. Zhou, J. J. Lin, B. Zhang and K. Liu, *J. Phys. Chem. A*, 2004, **108**, 7832–7836.
18 H. A. Bechtel, J. P. Camden, D. J. A. Brown, M. R. Martin, R. N. Zare and K. Vodopyanov, *Angew. Chem., Int. Ed.*, 2005, **44**, 2382–2385.
19 G. Czakó, Q. Shuai, K. Liu and J. M. Bowman, *J. Chem. Phys.*, 2010, **133**, 131101.
20 F. Wang and K. Liu, *J. Phys. Chem. Lett.*, 2011, **2**, 1421–1425.
21 B. Zhang, K. Liu, G. Czakó and J. M. Bowman, *Mol. Phys.*, 2012, **110**, 1617–1626.
22 F. Wang and K. Liu, *J. Phys. Chem. A*, 2013, **117**, 8536–8544.
23 J. Sansón, J. C. Corchado, C. Rangel and J. Espinosa-García, *J. Phys. Chem. A*, 2006, **110**, 9568–9574.
24 D. J. Donaldson, J. Parsons, J. J. Sloan and A. Stolow, *Chem. Phys.*, 1984, **85**, 47–62.
25 D. J. Donaldson, J. J. Sloan and J. D. Goddard, *J. Chem. Phys.*, 1985, **82**, 4524–4536.
26 J. D. Goddard, D. J. Donaldson and J. J. Sloan, *Chem. Phys.*, 1987, **114**, 321–329.
27 H. Feng, W. Sun, Y. Xie and H. F. Schaefer, *Chem. – Asian J.*, 2011, **6**, 3152–3156.
28 A. S. Manocha, D. W. Setser and M. A. Wickramaaratchi, *Chem. Phys.*, 1983, **76**, 129–146.
29 C. Walther and H. G. Wagner, *Berichte der Bunsengesellschaft für physikalische Chemie*, 1983, **87**, 403–409.
30 S. Wategaonkar and D. W. Setser, *J. Chem. Phys.*, 1987, **86**, 4477–4487.
31 A. Persky, *Chem. Phys. Lett.*, 2007, **439**, 3–7.
32 C. Xiao, G. Shen, X. Wang, H. Fan and X. Yang, *J. Phys. Chem. A*, 2010, **114**, 4520–4523.
33 J. Espinosa-García and J. C. Corchado, *J. Phys. Chem. A*, 1997, **101**, 7336–7344.
34 J. Espinosa-García and M. Monge-Palacios, *J. Phys. Chem. A*, 2011, **115**, 13759–13763.
35 J. Espinosa-Garcia, A. Fernandez-Ramos, Y. V. Suleimanov and J. C. Corchado, *J. Phys. Chem. A*, 2014, **118**, 554–560.
36 L. Tian, Y. Zhu, H. Song and M. Yang, *Phys. Chem. Chem. Phys.*, 2019, **21**, 11385–11394.
37 L. M. Raff, R. Komanduri, M. Hagan and S. T. S. Bukkapatnam, *Neural Networks in Chemical Reaction Dynamics*, Oxford University Press, Oxford, 2012.
38 B. Jiang and H. Guo, *J. Chem. Phys.*, 2013, **139**, 054112.
39 K. Shao, J. Chen, Z. Zhao and D. H. Zhang, *J. Chem. Phys.*, 2016, **145**, 071101.
40 H. Song, M. Yang and H. Guo, *J. Chem. Phys.*, 2016, **145**, 131101.
41 Z. Zhang, F. Gatti and D. H. Zhang, *J. Chem. Phys.*, 2019, **150**, 204301.
42 R. S. Judson, D. J. Kouri, D. Neuhauser and M. Baer, *Phys. Rev. A: At., Mol., Opt. Phys.*, 1990, **42**, 351–366.
43 D. H. Zhang and J. Z. H. Zhang, *J. Chem. Phys.*, 1994, **101**, 1146–1156.
44 D. Neuhauser, *J. Chem. Phys.*, 1994, **100**, 9272–9275.
45 J. Z. H. Zhang, *Theory and Application of Quantum Molecular Dynamics*, World Scientific, Singapore, 1999.
46 M. Yang, *J. Chem. Phys.*, 2008, **129**, 064315.
47 Q. Hu, H. Song, C. J. Johnson, J. Li, H. Guo and R. E. Continetti, *J. Chem. Phys.*, 2016, **144**, 244311.
48 R. N. Zare, *Angular Momentum*, Wiley, New York, 1988.
49 R. T. Pack, *J. Chem. Phys.*, 1974, **60**, 633–639.
50 P. McGuire and D. J. Kouri, *J. Chem. Phys.*, 1974, **60**, 2488–2499.
51 J. A. Fleck, Jr., J. R. Morris and M. D. Feit, *Appl. Phys.*, 1976, **10**, 129–160.
52 D. Neuhasuer and M. Baer, *J. Chem. Phys.*, 1989, **90**, 4351–4355.

53 W. H. Miller, S. D. Schwartz and J. W. Tromp, *J. Chem. Phys.*, 1983, **79**, 4889–4898.
54 D. H. Zhang and J. Z. H. Zhang, *J. Chem. Phys.*, 1993, **99**, 5615–5618.
55 J. V. Lill, G. A. Parker and J. C. Light, *Chem. Phys. Lett.*, 1982, **89**, 483–489.
56 J. Echave and D. C. Clary, *Chem. Phys. Lett.*, 1992, **190**, 225–230.
57 W. L. Hase, R. J. Duchovic, X. Hu, A. Komornicki, K. F. Lim, D.-H. Lu, G. H. Peslherbe, K. N. Swamy, S. R. Vande Linde, A. Varandas, H. Wang and R. J. Wolf, *Quantum Chem. Program Exch. Bull.*, 1996, **16**, 43.
58 C. Qu and J. M. Bowman, *J. Phys. Chem. A*, 2016, **120**, 4988–4993.
59 M. C. Gutzwiller, *Chaos in Classical and Quantum Mechanics*, Springer, New York, 1990.
60 C. Rangel, J. C. Corchado and J. Espinosa-García, *J. Phys. Chem. A*, 2006, **110**, 10375–10383.
61 J. C. Corchado and J. Espinosa-Garcia, *Phys. Chem. Chem. Phys.*, 2009, **11**, 10157–10164.
62 L. Ping, L. Tian, H. Song and M. Yang, *J. Phys. Chem. A*, 2018, **122**, 6997–7005.
63 D. G. Truhlar and J. T. Muckerman, *Atom-Molecule Collision Theory*, ed. R. B. Bernstein, Plenum, New York, 1979.
64 L. Bonnet and J. Espinosa-García, *J. Chem. Phys.*, 2010, **133**, 164108.
65 G. Czakó and J. M. Bowman, *J. Chem. Phys.*, 2009, **131**, 244302.
66 W. N. Olmstead and J. I. Brauman, *J. Am. Chem. Soc.*, 1977, **99**, 4219–4228.
67 C. H. DePuy, S. Gronert, A. Mullin and V. M. Bierbaum, *J. Am. Chem. Soc.*, 1990, **112**, 8650–8655.
68 Y. Xu, B. Xiong, Y. C. Chang and C. Y. Ng, *J. Chem. Phys.*, 2012, **137**, 241101.
69 Y. Xu, B. Xiong, Y. C. Chang and C. Y. Ng, *J. Chem. Phys.*, 2013, **139**, 024203.
70 S. G. Ard, A. Li, O. Martinez, N. S. Shuman, A. A. Viggiano and H. Guo, *J. Phys. Chem. A*, 2014, **118**, 11485–11489.
71 I. Szabó and G. Czakó, *J. Phys. Chem. A*, 2015, **119**, 12231–12237.
72 H. Song, A. Li, H. Guo, Y. Xu, B. Xiong, Y. C. Chang and C. Y. Ng, *Phys. Chem. Chem. Phys.*, 2016, **18**, 22509–22515.
73 H. Song, A. Li and H. Guo, *J. Phys. Chem. A*, 2016, **120**, 4742–4748.

